

# Transition-Metal Pentatelluride $\text{ZrTe}_5$ and $\text{HfTe}_5$ : a Paradigm for Large-gap Quantum Spin Hall Insulators

Hongming Weng, Xi Dai,<sup>\*</sup> and Zhong Fang<sup>†</sup>

*Beijing National Laboratory for Condensed Matter Physics,  
and Institute of Physics, Chinese Academy of Sciences, Beijing 100190, China;*

(Dated: October 1, 2013)

## Abstract

Quantum spin Hall (QSH) insulators, a new class of quantum matters, can support topologically protected helical edge modes inside bulk insulating gap, which can lead to dissipationless transport. A major obstacle to reach wide application of QSH is the lack of suitable QSH compounds, which should be easily fabricated and has large size of bulk gap. Here we predict that single layer  $\text{ZrTe}_5$  and  $\text{HfTe}_5$  are the most promising candidates to reach the large gap QSH insulators with bulk direct (indirect) band gap as large as 0.4 eV (0.1 eV), and robust against external strains. The 3D crystals of these two materials are good layered compounds with very weak inter-layer bonding and are located near the phase boundary between weak and strong topological insulators, which pave a new way to future experimental studies on both QSH effect and topological phase transitions.

## I. INTRODUCTION

Topological insulators (TI)<sup>1,2</sup> can support gapless boundary states inside bulk insulating gap, which are topologically protected and robust against perturbations. Particularly in two-dimensional (2D) TIs, namely the QSH insulators<sup>3,4</sup>, the low energy (back) scattering of the edge states is prohibited by the time reversal symmetry, leading to the dissipationless transport edge channels and the QSH effect<sup>5</sup>. However, the known experimental verifications of QSH effect in HgTe/CdTe<sup>6</sup> and InAs/GaSb<sup>7</sup> quantum well structures require extreme conditions, such as the precisely controlled molecular-beam-epitaxy (MBE) and the ultra low temperature (due to the small bulk band gap of the order of meV), which greatly obstruct the further experimental studies and possible applications.

To be a "good" QSH insulator, the material must meet the following important criteria: (1) It must be a good layered materials to get the 2D system easily; (2) It must have large 2D bulk band gap to realize the QSH effect at high temperature. The first proposal for the QSH insulator in graphene<sup>3</sup> is practically useless due to its extremely small gap ( $10^{-3}$ meV) induced by spin-orbit coupling (SOC)<sup>8</sup>, although graphene is so far the best 2D material which can be made easily even by scotch tape<sup>9</sup>. Recently Bi<sub>2</sub>TeI has been proposed to be another candidate for QSH insulator<sup>10</sup>, but its energy gap is also small. The Bismuth (111)-bilayer is potentially a large-gap (about 0.2 eV) QSH insulator<sup>11</sup>, however, it is inter-layer strongly bonded and its fabrication is hard (not experimentally achieved yet). Several other proposals, such as the ultra thin tin films<sup>12</sup> and the Cd<sub>3</sub>As<sub>2</sub> quantum well<sup>13</sup>, have the same problem. Since they are not layered materials, the well controlled MBE technique is required to obtain the ultra thin film samples.

Here we report that simple binary ZrTe<sub>5</sub> and HfTe<sub>5</sub>, previously known as layered thermoelectric compounds, are inter-layer weakly bonded comparable to that of graphite. Their single layer sheets, which can be made in principle with no need for MBE, are QSH insulators with large bulk gap, and robust against the lattice distortions. Therefore, ZrTe<sub>5</sub> and HfTe<sub>5</sub> are the most promising 2D TI, which satisfy both the above conditions and pave a new way to more experimental studies on QSH effect. Moreover, our calculations show that their three dimensional (3D) crystals formed by the stacking of layers are located in the vicinity of a transition between strong and weak TI, which further makes it a perfect platform to study the topological quantum phase transitions.

## II. COMPUTATIONAL METHODS

The *ab initio* calculations have been done by using the all electron full potential linearized augmented plane wave method implemented in the WIEN2k package<sup>31</sup> within the general gradient approximation (GGA). The choice of parameters, such as sampling of Brillouin Zone and cut-off of augmented plane waves, are carefully checked to ensure the convergence. The spin-orbit coupling (SOC) is included self-consistently within the second variational method. The inter-layer binding energy, i.e., the unit area total-energy difference between the single layer sheet and the 3D bulk, is calculated by using the local density approximation (LDA) of Perdew and Wang type exchange correlation<sup>32</sup>. It is known that LDA can give the Van der Waals type inter-layer coupling energy reasonably well<sup>33</sup>. The maximally localized Wannier functions (MLWF) for Te *p* orbitals have been constructed by using home made code<sup>34</sup> based on OpenMX<sup>35</sup>, which can reproduce the band structures calculated from the first-principles quite well. The surface and edge states have been calculated for slabs by using a tight-binding model constructed from the MLWFs generated above.

## III. RESULTS

### A. Layered crystal structure

Both  $\text{ZrTe}_5$  and  $\text{HfTe}_5$  take the same structure and have very similar properties. They have been shown to possess interesting electrical transport properties, such as the giant resistivity anomaly<sup>14,15</sup> and the large thermopower<sup>16,17</sup>. They crystallize in the orthorhombic layered structure<sup>18</sup> with space group  $Cmcm$  ( $D_{2h}^{17}$ ) as shown in Fig. 1 (hereafter we take  $\text{ZrTe}_5$  as an example). Trigonal prismatic chains of  $\text{ZrTe}_3$  (marked by red dashed line) run along the *a* axis, and these prismatic chains are linked via parallel zigzag chains of Te atoms along the *c* axis to form 2D sheet of  $\text{ZrTe}_5$  in the *a-c* plane. The sheets of  $\text{ZrTe}_5$  stack along the *b* axis, forming layered structure. The prism of  $\text{ZrTe}_3$  is formed by a dimer of  $\text{Te}_{1,2}^d$  atoms (with superscript *d* indicating the dimer and subscript 1,2 numbering the atoms) and one apical  $\text{Te}^a$  atom (with *a* meaning the apical), while the zigzag chain is formed by two  $\text{Te}_{1,2}^z$  atoms (with *z* indicating the zigzag chain). The primitive unit cell contains two formula units with two prisms and two zigzag chains. The corresponding subscripts numbering the atoms should be doubled.

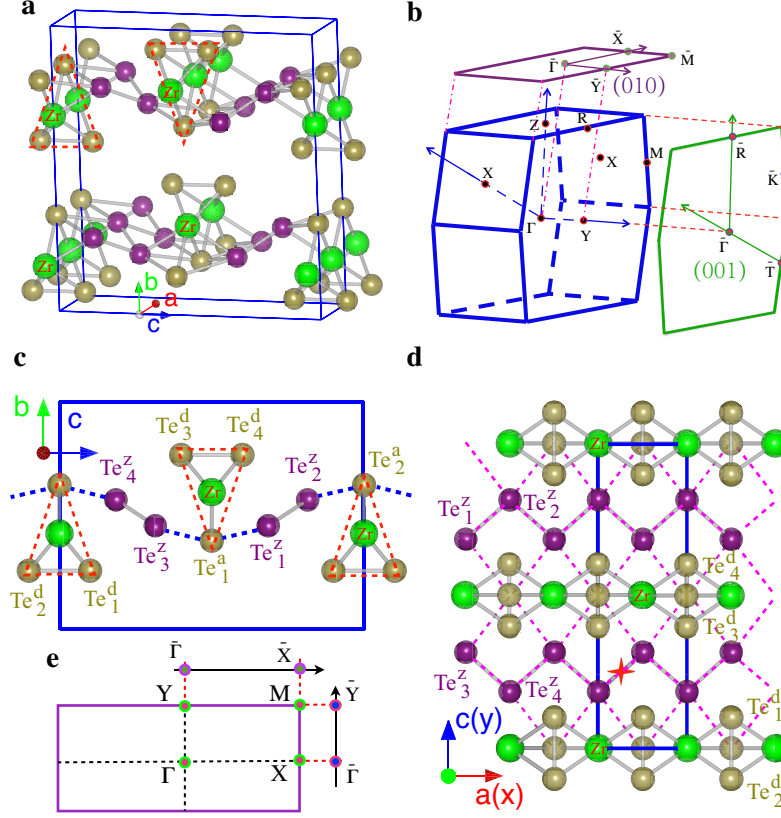


FIG. 1: (a) The crystal structure and (b) the bulk Brillouin Zone (BZ) and the projected surface BZ of 3D  $\text{ZrTe}_5$  ( $\text{HfTe}_5$ ). (c), (d) and (e) is the side view, top view, and BZ of single layer structure, respectively. In (d), the inversion center is indicated by the red star symbol, and the waved grid of Te square lattice sheet is shown as the pink dotted lines.

$\text{ZrTe}_5$  shows strong quasi-2D anisotropy<sup>19</sup>. The prism chains and zigzag chains are connected through the apical Te atoms, and the Te-Te bond length between two chains is just about 0.4 Å longer than that in the zigzag chain. If the Zr and  $\text{Te}^d$  dimer atoms are neglected, the remaining apical  $\text{Te}^a$  and zigzag  $\text{Te}^z$  atoms can be viewed as a waved grid of Te square lattice sheet (see Fig.1(d)), leading to a stable quasi-2D structure. Each  $\text{ZrTe}_5$  layer is nominally charge neutral, and the inter-layer distance (along  $b$  axis) is quite large (about 7.25 Å), suggesting the weak inter-layer coupling of presumably Van der Waals type. We have calculated the inter-layer binding energies for different compounds by using the first-principles total energy method (see method). The results shown in Fig. 2 suggest that the inter-layer binding energy of  $\text{ZrTe}_5$  or  $\text{HfTe}_5$  is as weak as that of graphite, and is much smaller than that of  $\text{Bi}_2\text{Se}_3$  and Bi (111)-bilayer. Given the easy procedure of making

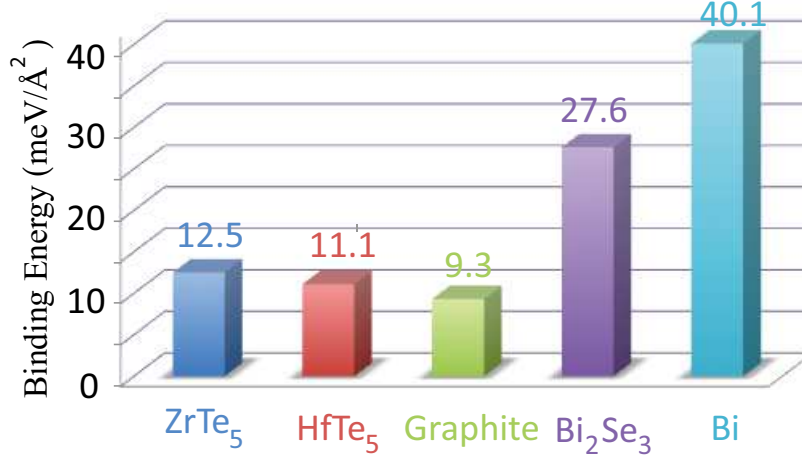


FIG. 2: The calculated inter-layer binding energies for several typical layered compounds.

graphene from graphite simply by scotch tape<sup>9</sup>, the comparably weak inter-layer binding energy suggests that the single layer of ZrTe<sub>5</sub> (or HfTe<sub>5</sub>) may be formed in a similar simple and efficient method.

### B. 2D Quantum Spin Hall Insulator

We now focus on the single layer of ZrTe<sub>5</sub> in the  $a$ - $c$  plane. Its structure is fully optimized by theoretical calculation. It is found that the relaxed lattice constants ( $a=4.036$  Å and  $c=13.843$  Å) and the internal atomic coordinates are all very close to their 3D bulk experimental values (less than one percent difference)<sup>18</sup>, again suggesting the stability of the single layer sheet. The calculated density of states shown in Fig. 3(a) suggest that the Zr-4*d* states are mostly unoccupied above the Fermi level, leading to the nearly ionic Zr<sup>4+</sup> state (by transferring  $\sim 4$  electrons onto the neighboring Te atoms). The states near the Fermi level are dominantly from the covalently bonded Te-5*p* states.

For the convenience of discussions, hereafter we define our coordinate system with  $x$ ,  $y$  being along the  $a$  and  $c$ -axis, respectively, and  $z$  being out of the 2D plane. We choose the origin of the coordinate system to be located on the Zr site. The calculated band structures for a single layer ZrTe<sub>5</sub> are shown in Fig. 3 (b) and (c). In the case without SOC, the system is a semimetal with a band-crossing along the  $\Gamma$ -X direction, implying the existence of band inversion around the  $\Gamma$ . The band crossing is unavoidable because the two bands belong to different representations distinguished by the  $m_{xz}$  symmetry along the

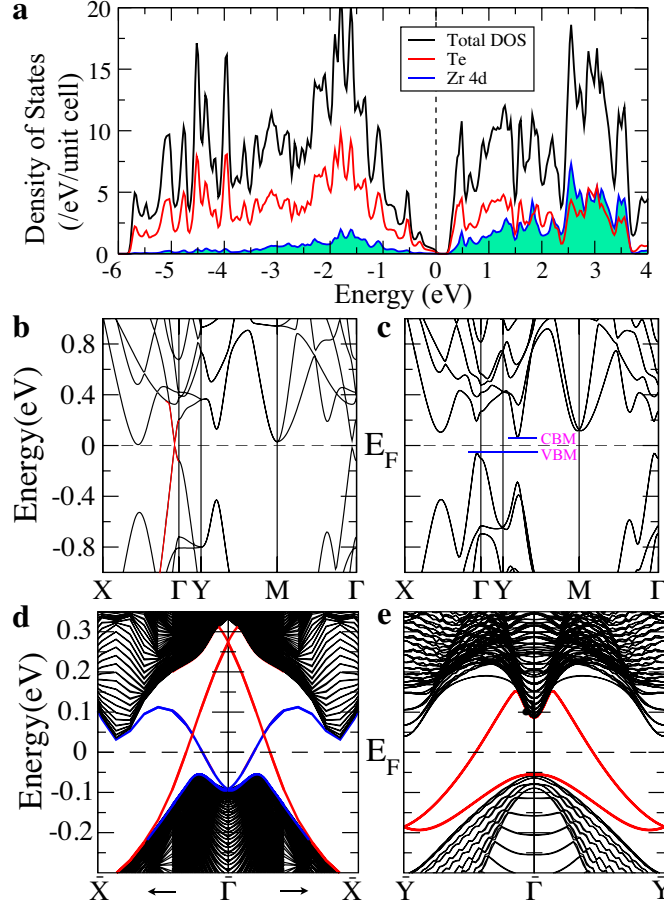


FIG. 3: The calculated electronic structures of single layer ZrTe<sub>5</sub>. (a) The density of states; (b) and (c) the band structures without and with SOC, respectively. The valence band maximum (VBM) and conduction band minimum (CBM) defining the in-direct band gap is indicated in (c); (d) and (e) are the calculated edge states for the  $x$ - and  $y$ -edges, respectively (see the main text for details).

$\Gamma$ -X axis. The inclusion of SOC will, however, mix them and open up a gap, resulting in an insulator with large direct (indirect) band gap of 0.4 eV (0.1 eV). We have checked the  $Z_2$  topological invariant<sup>3</sup> of the resulting insulating state by evaluating the parity eigen values of occupied states at four time-reversal-invariant-momenta (TRIM) points of the Brillouin Zone (BZ)<sup>20</sup>, and conclude that it is a non-trivial QSH insulator with  $Z_2=1$ . Since the band gap is mostly determined by SOC strength, we wouldn't expect much error bar of GGA type calculations (as it usually does for conventional semiconductors). Indeed, we have checked the electronic structure by using the hybrid functional HSE06,<sup>21</sup> as well as the modified

Becke-Johnson (mBJ) potential<sup>22</sup>. Both of them give the similar band gap with the band topology unchanged.

The 2D non-trivial insulating state in single layer  $\text{ZrTe}_5$  should support topologically protected conducting edge states. Two idea edges along the  $x$ - and  $y$ -direction are studied by tight-binding slab models (see method). The termination is between the prism chain and the zigzag chain for the former, and is between the two  $\text{Te}^z$  atoms of the zigzag chain for the later. The results are shown in Fig. 3(d) and (e). For the case of cutting along the  $x$  direction, the left and right edges of our slab are not symmetric, which leads to two separated Dirac cones at  $\bar{\Gamma}$ : one for the edge with prism chain termination (red), and other one for the zigzag chain termination (blue). While for the case of cutting along the  $y$  direction, both sides of the slab are symmetric and two Dirac cones (located at opposite sides) are energetically degenerate. There is another difference between  $x$ - and  $y$ -edge. The Dirac cones are at  $\bar{\Gamma}$  in the former, while at  $\bar{Y}$  in the later.

### C. Band inversion mechanism

The band inversion in single layer  $\text{ZrTe}_5$  is not due to SOC, instead it is mainly due to the non-symmorphic features of the space group. Therefore the physics of band inversion here can be understood without SOC, and the only effect of SOC is to open a energy gap afterwards. We note that the space group of the system is  $P_{mmn} (D_{2h}^{13})$ , which is a non-symmorphic one with the inversion center located not at the origin but at  $(1/4, 1/4)$ . As an important consequence of such space group symmetry, the eigenstates at all zone boundary TRIM points (namely, X, Y, and M) are all four-fold degenerate (including spin degrees of freedom) with two of them having even parity and the other two odd parity. This is because that at all the three zone boundary points the inversion operation anti-commutes with two important mirror operators  $m_{xz}$  and  $m_{yz}$ . (see detail in Appendix). The equal number of parities guarantees that any band inversion at those zone boundary TRIM points will not change the topology of the system and the  $Z_2$  index of the material is fully determined by the energy order of the bands at the  $\Gamma$  point, where only the Kramer degeneracy holds. We further notice that the mirror symmetry  $m_{yz}$  will transfer all the atoms into themselves. Therefore, the atomic  $p$  orbitals can be classified into two classes, namely, the  $p_x$  orbital and the  $p_{y/z}$  orbital, because they will not mix in the eigenstates of  $\Gamma$  point (in the absence of

SOC).

Our calculations suggest that the band inversion at  $\Gamma$  happens between the zigzag chain  $\text{Te}^z\text{-}p_x$  and the prism chain dimer  $\text{Te}^d\text{-}p_y$  states, as shown schematically in Fig. 4. At the atomic limit, they are all four-fold degenerated since there are four equivalent Te atoms for each class. The strong intra-chain covalence bonding will split them into double degenerate bonding and anti-bonding states, respectively, and then the weak inter-chain coupling will further split them into singly degenerate states. It is important to note the symmetry difference between the two chains. The two dimer  $\text{Te}_{1,2}^d$  atoms in the same prism chain are related by the mirror  $m_{xz}$  symmetry, while the two  $\text{Te}_{1,2}^z$  atoms in the same zigzag chain are related by the inversion symmetry. The bonding and antibonding states caused by the intra-chain coupling can therefore be distinguished by the eigenvalues  $m_{xz}=\pm 1$  for the former, and the parity  $p=\pm 1$  for the later. Due to the strong intra-chain coupling, the band inversion is introduced between the bonding  $\text{Te}^d$  states with  $m_{xz}=1$  and the antibonding  $\text{Te}^z$  states with  $p=-1$ , as illustrated in Fig. 4. Within the two bonding  $\text{Te}^d$  states of  $m_{xz}=1$ , only one state has odd parity. As a result, its occupation changes the total parity of the occupied states at  $\Gamma$ , which leads to the QSH state.

#### D. Strain effects

We emphasize that, unlike the situation in typical TI such as the  $\text{Bi}_2\text{Se}_3$  family compounds<sup>23</sup>, the band inversion in  $\text{ZrTe}_5$  single layer is not due to SOC, instead it is due to the special non-symmorphic space group features as discussed above. As long as the inter-chain coupling is not strong enough to reverse the band ordering again (between the ( $m_{xz}=-1$ ,  $p=+1$ ) state and the ( $m_{xz}=1$ ,  $p=-1$ ) state, as shown in Fig. 4), the QSH state should be stable. We have checked the stability of this QSH state as function of strains. Without lost of generality, here we assume that the lattice parameters  $a$  and  $c$  are equally scaled by possible external potentials, and for each fixed volume we fully optimize the internal coordinates. The results shown in Fig. 5 suggest that the QSH state survives even if the volume is expanded by more than 20% or compressed by 10%, indicating its robust stability against the strains. This makes it highly adaptable in various application environments. In the case of compressing, the too much enhanced inter-chain coupling will finally kill the QSH state, as discussed above.



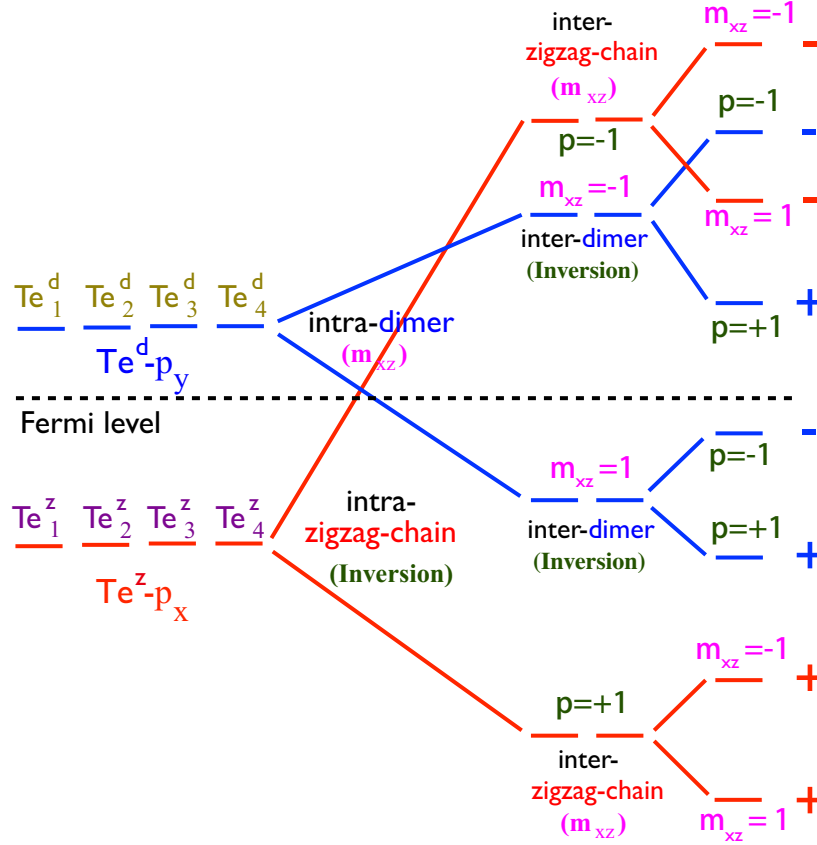


FIG. 4: The schematic illustration of the band inversion mechanism (see main text for details).

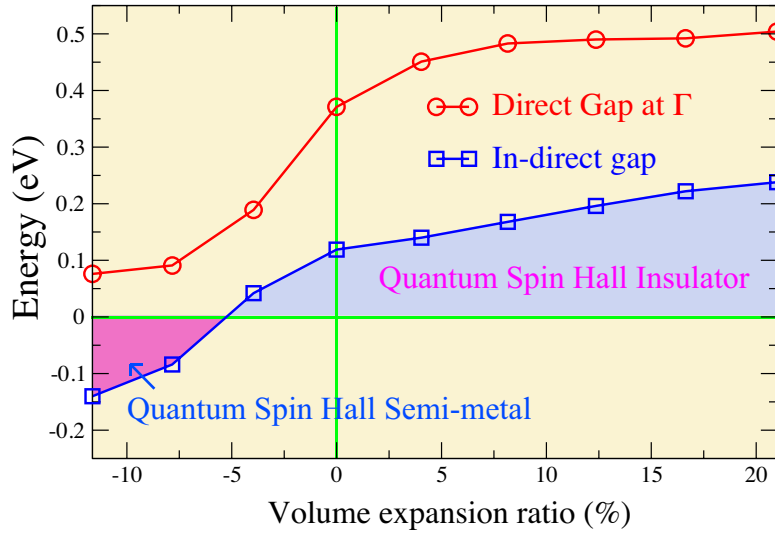


FIG. 5: The calculated band gaps of single layer  $\text{ZrTe}_5$  as function of volume change. Both the direct gap at  $\Gamma$  and the in-direct band gap are shown. The non-trivial  $Z_2$  topology survives as long as the band gap at  $\Gamma$  remains positive.

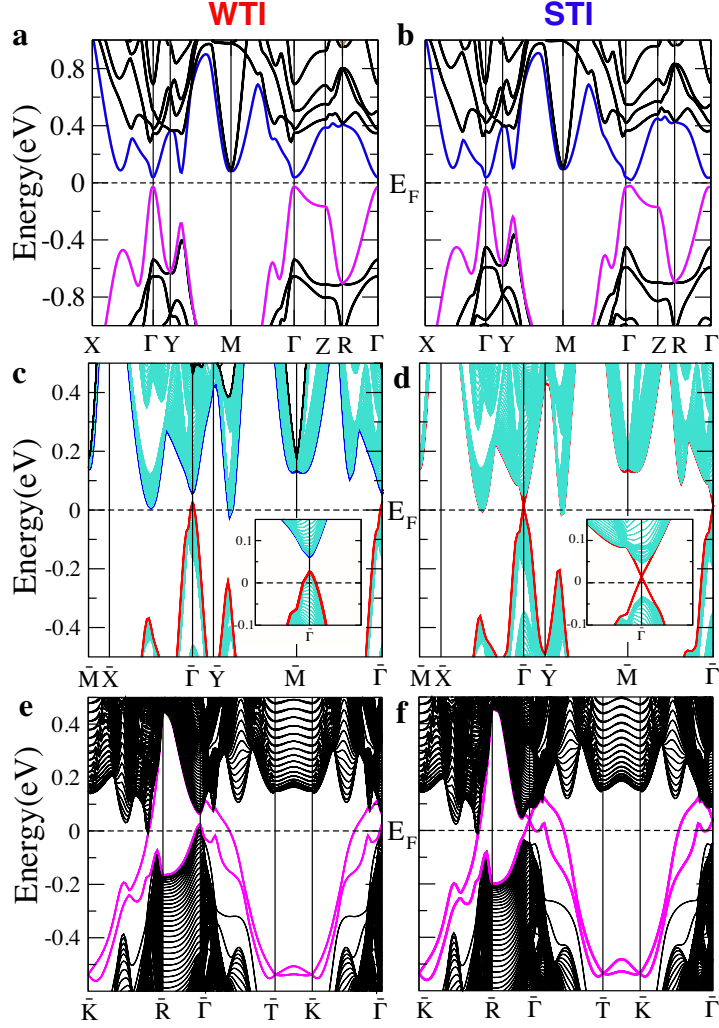


FIG. 6: The calculated band structures and surface states for the 3D  $\text{ZrTe}_5$ . (a) and (b) are for the bulk, (c) and (d) are for the top surface, and (e) and (f) are for the side surfaces as indicated in Fig. 1. The weak TI (WTI) solutions (left panels) are obtained by using optimized lattice parameters, while the strong TI (STI) solutions (right panels) are from the experimental ones. (see main text for details).

### E. 3D weak and strong TI

Given the QSH state in single layer  $\text{ZrTe}_5$ , it is important to check if the stacked 3D compound is a weak or a strong TI<sup>24</sup>. Interestingly, if we use the experimental lattice parameters<sup>18</sup>, we get a 3D strong TI with topological invariant (1; 001); however, if the optimized lattice parameters, which are only about 2% larger than experimental ones, are

used, we get a 3D weak TI state<sup>25</sup> with topological invariant (0; 001). The difference between two solutions are due to the tiny overlap of the states at the  $\Gamma$  point of 3D BZ, which inverse the parity (see Fig. 6). If we use the mBJ potential<sup>22</sup> instead of GGA for the above two calculations, we get both strong TI solutions. We have to conclude that the required accuracy to distinguish these two states for reality is beyond the ability of our present calculations. Nevertheless, our results suggest that the 3D compound is located very close to the boundary between the weak and strong TI, which provides us an excellent opportunity to study the topological phase transition experimentally. In Fig. 6, we show the calculated band structures and the surface states of both strong and weak TI solutions. Odd number of Dirac cones, one for the top- and three for the side-surface, are obtained in the strong TI phase. For the weak TI case, however, even number of Dirac cones, none for the top- and two for the side surface, are obtained. It will be very interesting to observe such topological phase transition in experiments just simply pressing or stretching the sample along the layer stacking direction. It will be also heuristic to see whether the long standing mysterious giant resistivity anomaly<sup>14,15</sup> observed in both  $\text{ZrTe}_5$  and  $\text{HfTe}_5$  has anything to do with the possible weak to strong TI phase transition.

#### IV. DISCUSSION

Finally, we have performed all the calculations for  $\text{HfTe}_5$  and draw the same conclusions as  $\text{ZrTe}_5$ . Their 2D and 3D band structures and size of band gap are all very similar. It is experimentally known that the transition metal site Zr or Hf can be substituted by many other elements, such as rare earth, which even shows precursor of possible magnetic ordering<sup>17</sup>. The breaking of time reversal symmetry (TRS) will allow us to study the possible quantum anomalous Hall effect<sup>26,27</sup>. Moreover, due to the strong 2D features of these materials, the edge states will appear not only at the edge of the single-layer samples but also at the terrace edges on the top surface of the 3D materials. When such terrace edges are covered by a s-wave superconducting layer, 1D topological superconductors with Majorana bound states at the end of the terrace edges will be induced by the superconducting proximity effect<sup>28-30</sup>.

## V. ACKNOWLEDGEMENTS

We acknowledge the supports from the NSF of china and the 973 program of China (No. 2011CBA00108 and 2013CBP21700).

## VI. APPENDIX

In this appendix, we prove that for single layer  $\text{ZrTe}_5$  the energy bands at all the zone boundary TRIM points are at least doubly degenerate with opposite parity. For simplicity, we neglect the spin degree of freedom and the conclusion can be easily generalized to the spin-1/2 case. Since the energy bands of  $\text{ZrTe}_5$  near the Fermi level are formed by Te 5p-orbitals, the Wannier functions centered at each atomic sites with particular atomic feature (like  $p_x$ ,  $p_y$  and  $p_z$ ) carry a natural representation for the space group. First we define the following Wannier basis in the momentum space,

$$\phi_{\alpha k}^{\mu}(r) = \frac{1}{\sqrt{N}} \sum_i \phi_{\alpha}(r - \tau_{\mu} - R_i) e^{ik(R_i + \tau_{\mu})}$$

, where  $i$  is the unit cell index,  $\mu$  denotes the different atomic positions in a unit cell and  $\alpha$  labels different orbitals on a same atomic position. When a general space group operator  $\{P_R | t_R\}$ , with  $P_R$  and  $t_R$  representing the rotation and translation part of the operator respectively, acts on the Wannier basis, we have

$$\begin{aligned} \{P_R | t_R\} \phi_{\alpha k}^{\mu}(r) &= t_R (P_R \phi_{\alpha k}^{\mu}(r)) \\ &= \frac{1}{\sqrt{N}} \sum_{i'} \phi_{\mathcal{R}\alpha}(r - t_R - \mathcal{R}\tau_{\mu} - R_{i'}) e^{i(\mathcal{R}k)(R_{i'} + \mathcal{R}\tau_{\mu})} \\ &= \frac{1}{\sqrt{N}} \sum_{i'\alpha'\mu'} \phi_{\alpha'}(r - R_0^{\mu} - \tau_{\mu'} - R_{i'}) e^{i(\mathcal{R}k)(R_{i'} + R_0^{\mu} + \tau_{\mu'} - t_R)} \\ &= \phi_{\mathcal{R}\alpha, \mathcal{R}k}^{\mu'}(r) e^{-i(\mathcal{R}k)t_R} = \sum_{\alpha'\mu'} Z_{\mu\mu'}^{\mathcal{R}} O_{\alpha\alpha'}^{\mathcal{R}} \phi_{\alpha', \mathcal{R}k}^{\mu'}(r) e^{-i(\mathcal{R}k)t_R} \end{aligned}$$

where we have take  $t_R + \mathcal{R}\tau_{\mu} = R_0^{\mu} + \tau_{\mu'}$  and  $\alpha' = \mathcal{R}\alpha$ ,  $Z^{\mathcal{R}}$  and  $O^{\mathcal{R}}$  are matrices describing the transformation in atomic positions and orbitals respectively. We would emphasize that in the above equation  $\phi_{\alpha \mathcal{R}k}^{\mu}(r)$  does not necessary equal to  $\phi_{\alpha k}^{\mu}(r)$ , even when  $\mathcal{R}k = k + G_n$  with  $G_n$  representing a vector in reciprocal lattice. They can differ by a phase factor due to the specific choice of the gauge fixing condition here, which contains a phase factor  $e^{ik\tau_{\mu}}$  for

orbitals located at different atomic position  $\tau_\mu$ . Using the Wannier representation introduced above and choosing the Zr site as the origin of the coordinate frame, we pick two operators, inversion and mirror  $m_{yz}$ , which can be written as the following

$$\{I|\frac{1}{2}, \frac{1}{2}\} \text{ and } \{m_{yz}|0, 0\}$$

First we act  $\{I|\frac{1}{2}, \frac{1}{2}\} \cdot \{m_{yz}|0, 0\}$  to the Wannier basis, which lead to

$$\begin{aligned} & \{I|\frac{1}{2}, \frac{1}{2}\} \cdot \{m_{yz}|0, 0\} \phi_{\alpha k}^\mu(r) = \\ & [Z^I Z^{yz}]_{\mu\mu'} [O^I O^{yz}]_{\alpha, \alpha'} \phi_{\alpha'(Im_{yz}k)}^{\mu'}(r) e^{-i(Im_{yz}k)t_R} \end{aligned}$$

where we have  $t_R = \{\frac{1}{2}, \frac{1}{2}\}$ . And similarly when we act  $\{m_{yz}|0, 0\} \cdot \{I|\frac{1}{2}, \frac{1}{2}\}$ , we have

$$\begin{aligned} & \{m_{yz}|0, 0\} \cdot \{I|\frac{1}{2}, \frac{1}{2}\} \phi_{\alpha k}^\mu(r) \\ & = [Z^{yz} Z^I]_{\mu\mu'} [O^{yz} O^I]_{\alpha, \alpha'} \phi_{\alpha'(m_{yz}Ik)}^{\mu'}(r) e^{-i(Ik)t_R} \end{aligned}$$

Since we can easily prove that  $Z^{yz} Z^I = Z^I Z^{yz}$  and  $O^{yz} O^I = O^I O^{yz}$ , the only difference between the above two is the phase factor, which differs by  $-1$  for  $(\pi, 0)$  and  $(\pi, \pi)$ . Therefore for these two points we have  $\{I|\frac{1}{2}, \frac{1}{2}\} \cdot \{m_{yz}|0, 0\} = -\{m_{yz}|0, 0\} \cdot \{I|\frac{1}{2}, \frac{1}{2}\}$ . Because both the above symmetry operators commute with the Hamiltonian, we can easily prove that if  $\phi_k$  is eigen state of Hamiltonian with given parity, the state  $\{m_{yz}|0, 0\} \phi_k$  is another eigen state of Hamiltonian but with opposite parity. Therefore we have proved that at  $(\pi, 0)$  and  $(\pi, \pi)$ , all the states come in pairs with opposite parity. Replacing  $m_{yz}$  by another mirror  $m_{xz}$ , we can easily prove that another zone boundary TRIM point  $(0, \pi)$  has the same property. In conclusion, at all these zone boundary TRIM points, the eigen states always come in degenerate pairs with opposite parity.

## VII. AUTHOR CONTRIBUTIONS

H.M.W. did the material search and the first principle calculations. X.D. and Z.F. did the symmetry and topology analysis. All the authors contributed to the analysis of the computational data and writing the manuscript.

---

\* Electronic address: daix@aphy.iphy.ac.cn

<sup>†</sup> Electronic address: zfang@aphy.iphy.ac.cn

- <sup>1</sup> M. Z. Hasan, and C. L. Kane, *Colloquium: Topological insulators*, Rev. Mod. Phys. **82**, 3045 (2010).
- <sup>2</sup> X.-L. Qi, and S.-C. Zhang, *Topological insulators and superconductors*, Rev. Mod. Phys. **83**, 1057 (2011).
- <sup>3</sup> C. L. Kane, E. J. Mele, *Quantum spin hall effect in graphene*, Phys. Rev. Lett. **95**, 226801 (2005); *ibid*  $Z_2$  *Topological Order and the Quantum Spin Hall Effect*, Phys. Rev. Lett. **95**, 146802 (2005).
- <sup>4</sup> B. A. Bernevig, S. C. Zhang, *Quantum Spin Hall Effect*, Phys. Rev. Lett. **96**, 106802 (2006).
- <sup>5</sup> B. A. Bernevig, T. L. Hughes, S. C. Zhang, *Quantum spin hall effect and topological phase transition in HgTe quantum wells*, Science **314**, 1757 (2006);
- <sup>6</sup> M. König, S. Wiedmann, C. Brüne, A. Roth, H. Buhmann, L. W. Molenkamp, X. L. Qi, and S. C. Zhang, *Quantum spin hall insulator state in HgTe quantum wells*, Science **318**, 766 (2007);
- <sup>7</sup> I. Knez, R. R. Du, and G. Sullivan, *Evidence for Helical Edge Modes in Inverted InAs=GaSb Quantum Wells*, Phys. Rev. Lett. **107**, 136603 (2011).
- <sup>8</sup> Y. G. Yao, F. Ye, X. L. Qi, S. C. Zhang, Z. Fang, *Spin-orbit gap of graphene: First-principles calculations*, Phys. Rev. B **75**, 041401 (2007).
- <sup>9</sup> K. S. Novoselov, A. K. Geim, S. V. Morozov, D. Jiang, Y. Zhang, S. V. Dubonos, I. V. Grigorieva, and A. A. Firsov, *Electric field effect in atomically thin carbon films*, Science **306**, 666 (2004); A. K. Geim and K. S. Novoselov, *The rise of graphene*. Nat. Mat. **6**, (2007).
- <sup>10</sup> P. Tang, B. Yan, W. Cao, S.-C. Wu, C. Felser, and W. Duan, *Weak topological insulators induced by the inter-layer coupling: A first-principles study of stacked Bi<sub>2</sub>TeI*, arXiv: 1307.8054 (2013).
- <sup>11</sup> S. Murakami, *Quantum Spin Hall Effect and Enhanced Magnetic Response by Spin-Orbit Coupling*, Phys. Rev. Lett. **97**, 236805 (2006).
- <sup>12</sup> Y. Xu, B. H. Yan, H. J. Zhang, J. Wang, G. Xu, P. Z. Tang, W. H. Duan, S. C. Zhang, *Large-gap quantum spin Hall insulators in tin films*, arXiv: 1306.3008 (2013).
- <sup>13</sup> Z. J. Wang, H. M. Weng, Q. S. Wu, X. Dai, Z. Fang, *Three Dimensional Dirac Semimetal and Quantum Spin Hall Effect in Cd<sub>3</sub>As<sub>2</sub>*, arXiv: 1305.6780 (2013).
- <sup>14</sup> E. F. Skelton, T. J. Wieting, S. A. Wolf, W. W. Fuller, D. U. Gubser, and T. L. Francavilla, *Giant resistivity and X-ray diffraction anomalies in low-dimensional ZrTe<sub>5</sub> and HfTe<sub>5</sub>*, Solid State Commun. **42**, 1 (1982).

- <sup>15</sup> T. M. Tritt, N. D. Lowhorn, R. T. Littleton IV, A. Pope, C. R. Feger, and J. W. Kolis, *Large enhancement of the resistive anomaly in the pentatelluride materials  $\text{HfTe}_5$  and  $\text{ZrTe}_5$  with applied magnetic field*, Phys. Rev. B **60**, 7816 (1999).
- <sup>16</sup> W. W. Fuller, S. A. Wolf, T. J. Wieting, R. C. LaCoe, P. M. Chaikin, and C. Y. Huang, *Pressure effects in  $\text{HfTe}_5$  and  $\text{ZrTe}_5$* , J. Phys. Colloques **44**, C3-1709 (1983) .
- <sup>17</sup> N. D. Lowhorn, T. M. Tritt, E. E. Abbott, J. W. Kolis, *Enhancement of the power factor of the transition metal pentatelluride  $\text{HfTe}_5$  by rare-earth doping*, Appl. Phys. Lett. **88**, 022101 (2006).
- <sup>18</sup> H. Fjellvåg and A. Kjekshus, *Structural properties of  $\text{ZrTe}_5$  and  $\text{HfTe}_5$  as seen by powder diffraction*, Solid State Commun. **60**, 91(1986)
- <sup>19</sup> A. Smontara, K. Biljaković, M. Miljak and T. Sambong, *Thermal and magnetic measurements on  $\text{ZrTe}_5$* , Physica **143B** 267 (1986).
- <sup>20</sup> L. Fu, and C. L. Kane, *Topological insulators with inversion symmetry*, Phys. Rev. B **76**, 045302 (2007).
- <sup>21</sup> J. Heyd, G. E. Scuseria, and M. Ernzerhof, *Erratum: “Hybrid functionals based on a screened Coulomb potential”*[*J. Chem. Phys.* **118**, 8207 (2003)], J. Chem. Phys. **124**, 219906 (2006).
- <sup>22</sup> F. Tran, and P. Blaha, *Accurate Band Gaps of Semiconductors and Insulators with a Semilocal Exchange-Correlation Potential*, Phys. Rev. Lett. **102**, 226401 (2009).
- <sup>23</sup> H. J. Zhang, C.-X. Liu, X.-L. Qi, X. Dai, Z. Fang, and S.-C. Zhang, *Topological insulators in  $\text{Bi}_2\text{Se}_3$ ,  $\text{Bi}_2\text{Te}_3$  and  $\text{Sb}_2\text{Te}_3$  with a single Dirac cone on the surface*, Nature Phys. **5**, 438 (2009).
- <sup>24</sup> L. Fu, C. L. Kane, E. J. Mele, *Topological Insulators in Three Dimensions*, Phys. Rev. Lett. **98**, 106803 (2007).
- <sup>25</sup> B. Yan, L. Müchler, and C. Felser, *Prediction of Weak Topological Insulators in Layered Semiconductors*, Phys. Rev. Lett. **109**, 116406 (2012).
- <sup>26</sup> Rui Yu, Wei Zhang, Hai-Jun Zhang, Shou-Cheng Zhang, Xi Dai, and Zhong Fang, *Quantized Anomalous Hall Effect in Magnetic Topological Insulators*, Science **329**, 61 (2010).
- <sup>27</sup> C. Z. Chang, J. Zhang, X. Feng, J. Shen, Z. Zhang, M. Guo, K. Li, Y. Ou, P. Wei, L. Wang, Z. Q. Ji, Y. Feng, S. Ji, X. Chen, J. Jia, X. Dai, Z. Fang, S.-C. Zhang, K. He, Y. Wang, L. Lu, X. C. Ma, and Q. K. Xue, *Experimental Observation of the Quantum Anomalous Hall Effect in a Magnetic Topological Insulator*, Science, **340**, 167 (2013).
- <sup>28</sup> V. Mourik, K. Zuo, S. M. Frolov, S. R. Plissard, E. P. A. M. Bakkers, L. P. Kouwenhoven, *Signatures of Majorana Fermions in Hybrid Superconductor-Semiconductor Nanowire Devices*,

- Science **336**, 1003 (2012).
- <sup>29</sup> R. M. Lutchyn, J. D. Sau, S. Das Sarma, *Majorana fermions and a topological phase transition in semiconductor-superconductor heterostructures*, Phys. Rev. Lett. **105**, 077001 (2010).
  - <sup>30</sup> Y. Oreg, G. Refael, F. von Oppen, *Helical liquids and Majorana bound states in quantum wires*, Phys. Rev. Lett. **105**, 177002 (2010).
  - <sup>31</sup> P. Blaha, K. Schwarz, G. Madsen, D. Kvasnicka, & J. Luitz, *WIEN2k, An Augmented Plane Wave Plus Local Orbitals Program for Calculating Crystal Properties* (TU Vienna, Vienna, 2001).
  - <sup>32</sup> J. P. Perdew, and Y. Wang, *Accurate and simple analytic representation of the electron-gas correlation energy*, Phys.Rev. B **45**, 13244 (1992).
  - <sup>33</sup> H. Lind, S. Lidin, and U. Häussermann, *Structure and bonding properties of  $(\text{Bi}_2\text{Se}_3)_m(\text{Bi}_2)_n$  stacks by first-principles density functional theory*, Phys. Rev. B **72**, 184101 (2005).
  - <sup>34</sup> H. Weng, T. Ozaki, K. Terakura, *Revisiting magnetic coupling in transition-metal-benzene complexes with maximally localized Wannier functions*, Phys. Rev. B **79**, 235118 (2009).
  - <sup>35</sup> <http://www.openmx-square.org>